Experiments in Fluids 37 (2004) 128–136
DOI 10.1007/s00348-004-0792-4

Measurements of the gas and particle flow within a converging-diverging nozzle for high speed powdered vaccine and drug delivery

M. A. F. Kendall, N. J. Quinlan, S. J. Thorpe, R. W. Ainsworth, B. J. Bellhouse

Abstract A unique system has been developed based upon the concept of accelerating pharmaceutical agents in particle form with a gas flow to attain sufficient momentum to enter the epidermis of human skin and achieve a pharmacological endpoint. This paper presents an experimental investigation of the transient gas and particle dynamics within a transonic converging-diverging nozzle prototype. The primary gas flow regimes are identified through Pitot-static pressure surveys and schlieren images with a high frame rate. The action of the gas flow-field in imparting momentum to the drug particles is investigated through schlieren imaging and time-resolved Doppler global velocimetry (DGV).

Abbreviations

DGV	Doppler global velocimetry
CCD	Charge coupled device
CST	Contoured shock tube

1 Introduction

Intradermal powder injection is a novel technology for needle-free administration of a range of vaccines and drugs. Although liquid injection through needle and syringe is simple, versatile, inexpensive and widely used, it is disliked by many patients and entails risks of contamination and injury. Alternatives including liquid jet injectors, creams, diffusion patches and pulmonary systems have been developed with varied advantages and limitations. Intradermal powder injection is a relatively new needle-free technology, in which particles containing vaccines (and drugs) are accelerated to sufficient momentum to penetrate the skin and achieve a pharmacological effect. Sanford et al. (1990) pioneered this innovation with systems designed to deliver DNA coated metal particles (with diameter of the order of 1 μm) into plant cells for genetic modification using pistons accelerated along the barrels of adapted guns. The concept was extended by Bellhouse et al. (1994) to the treatment of humans with particles accelerated by entrainment in a supersonic gas flow. Prototype devices embodying this concept have been shown to be effective, painless, and applicable to pharmaceutical therapies ranging from protein delivery (Burkoth et al. 1999) to conventional (Chen et al. 2000) and DNA vaccines (Lesinski et al. 2001). Derivatives of these prototypes are in commercial development for clinical use in humans under the name Dermal PowderJect; an example is illustrated in Fig. 1.

To achieve the concept's full potential in a range of pharmaceutical applications, a thorough understanding of the gas-particle dynamics is required. Studies have been performed on simplified prototype systems to meet this end.

The first steps toward developing this understanding consisted of a measurement programme in which static pressures and time-integrated Doppler global velocimetry (DGV) measurements of drug particle velocity were acquired in a simplified device (Quinlan 1999; Quinlan et al. 2001). These measurements were useful, but gave an incomplete description of the predominantly unsteady flow in the device.

In this paper, the results of an extended experimental investigation of the transient gas and particle dynamics within a prototype intradermal particle delivery system are presented. The primary gas flow regimes are identified from Pitot-static pressure surveys and schlieren images. The action of the gas flow-field in imparting momentum to vaccine or drug particles is quantified with time-resolved DGV measurements. The experimental data are analysed collectively and lead to a discussion of the relative effects of different gas flow regimes on the particle momentum distribution throughout the nozzle. Finally, the implications of these findings for biological performance of the system and for the direction of future developments are discussed.

2 Device geometry and operating conditions

The focus of this study is on a prototype vaccine delivery system simpler in construction than the device used in clinical applications illustrated in Fig. 1. Key components

Received: 21 June 2002 / Accepted: 15 December 2003
Published online: 21 April 2004

M. A. F. Kendall (✉), S. J. Thorpe, R. W. Ainsworth, B. J. Bellhouse
Department of Engineering Science, University of Oxford, UK
E-mail: Mark.Kendall@eng.ox.ac.uk
Tel.: +44-865-274758
Fax: +44-1865-274754

N. J. Quinlan
Department of Mechanical and Biomedical Engineering,
National University of Ireland, Galway, Republic of Ireland

M.A.F Kendall and N.J. Quinlan contributed equally to this paper.

Some of this work was originally presented at the 22nd International Symposium on Shock Waves, Imperial College, London, UK.

The authors thank PowderJect Pharmaceuticals Plc for its support of this work, the EPSRC instrument loan pool for the Kodak HS4540 Camera, EPSRC grant GR/JS4307 for the DGV work and Terry Jones for making available schlieren equipment at the Southwell Laboratory within the University of Oxford.

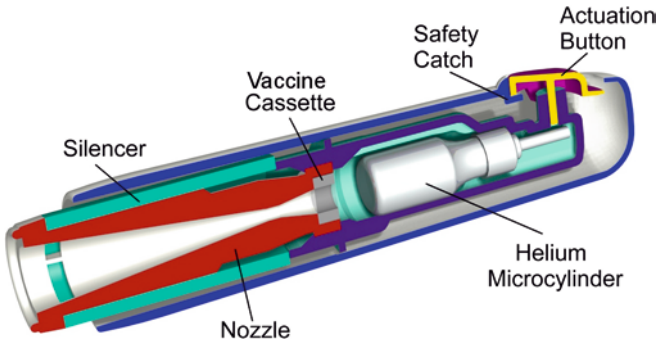

Fig. 1. Schematic of a commercially-oriented needle-free vaccine delivery system configured for clinical use in people

of the needle-free vaccine prototype under study are shown schematically in Fig. 2. Prior to operation, the gas canister is filled with helium to 6 MPa and the vaccine cassette, comprising two 20 μm diaphragms, is loaded with a powdered pharmaceutical payload of 0.5 to 5 mg. The pharmaceutical material is placed on the lower diaphragm surface. Operation commences when the valve in the gas canister is opened to release gas into the rupture chamber where the pressure builds up until the two diaphragms retaining the vaccine particles sequentially burst. The rupture of the downstream diaphragm initiates a shock which propagates down the converging-diverging nozzle. The ensuing expansion of stored gas results in a short-duration flow in which the drug particles are entrained and accelerated through the device. After leaving the device, particles impact on the skin and penetrate the skin to deliver a pharmacological effect. In clinical use, the prototype device would be typically fitted with a silencer and positioned with the nozzle exit plane 10 mm from the skin. In the research described here, the effects of both a silencer (such as in Fig. 1) and the target surface or skin (neither shown in Fig. 2) on the fluid dynamics of the whole system have not been considered.

3 Experimental techniques

3.1 Pitot and static pressure measurements

The prototype device was instrumented with wall-mounted pressure transducers with the aim of quantifying the gas flow-field. The gauges were used to measure the static pressure at various locations in the device. Within the canister (position p_1) and rupture chamber (p_2) piezoelectric PCB pressure transducers were used. More compact Kulite pressure transducers (Kulite Sensors, UK) were flush-mounted in the nozzle wall at 5 mm intervals between 3.5 and 38.5 mm upstream of the exit plane (Fig. 2).

The Pitot sensor consisted of a Kulite pressure transducer mounted in a probe with a 2 mm outer diameter. In each pressure measurement experiment, the Pitot probe was placed on the nozzle centreline at an axial location corresponding to that of a wall-mounted static pressure transducer. Experiments were carried out with and without the Pitot probe to determine the effect of the probe itself on the flow-field. It was found that the probe had no detectable effect over the time scales of interest (outlined in Fig. 5) at distances of up to 23.5 mm upstream of the nozzle exit plane.

3.2 Schlieren visualisation

The schlieren technique was primarily used to investigate the two-dimensional nature of the gas flow-field and, to a lesser extent, the gas flow-field's interaction with particles. The schlieren system had mirror focal lengths of 2.75 m. A Kodak HS4540 high speed Charge Coupled Device (CCD) camera was used to record up to 3000 schlieren images in each experiment at 9000 frames per second. The light source for the experiment was a copper-vapour laser (Oxford Lasers, UK) delivering 20 ns pulses in synchronisation with the CCD camera. To allow schlieren imaging inside the nozzle, a transparent square-section nozzle was constructed with the geometry outlined in Fig. 3. The axial variation of cross-sectional area in this nozzle was identical to that of the original (axisymmetric) Dermal PowderJect prototype nozzle (Fig. 2).

3.3 Doppler global velocimetry

The principles and details of the time-resolved DGV technique applied in this work are described in full elsewhere by Quinlan et al. (2001) and Thorpe et al. (2000), and only a very brief account is given here. In general, DGV is based on the use of a cell filled with iodine vapour as a frequency-dependent light absorption

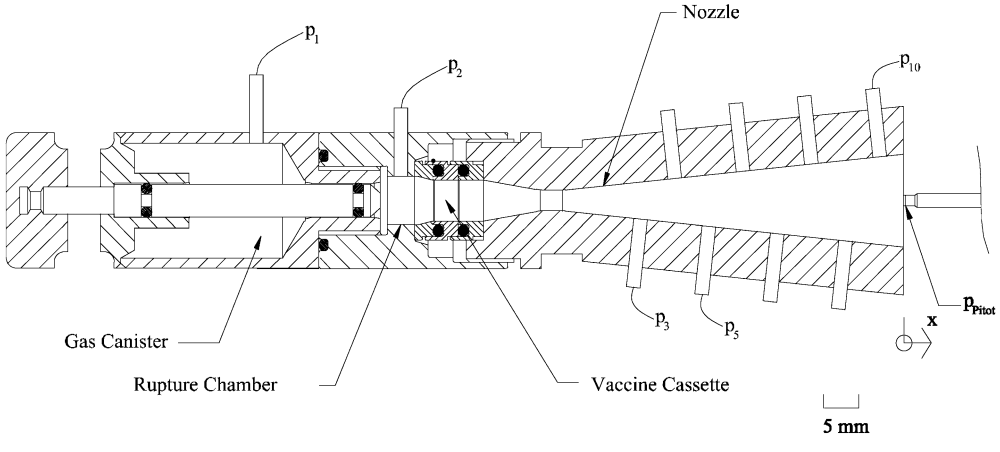

Fig. 2. Schematic of a simplified prototype vaccine device instrumented for Pitot and static pressure measurements. The static pressure transducers are labelled p_1–p_{10}

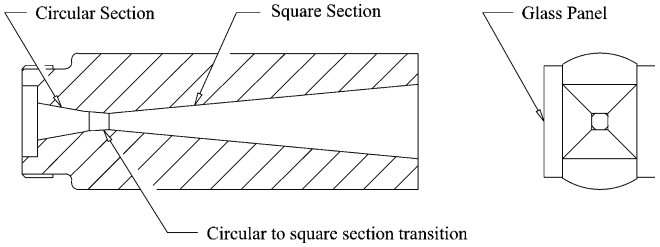

Fig. 3. Schematic of the circular-to-square section nozzle for the schlieren experiments

filter to measure the Doppler shift in light which is scattered by moving particles. The flow-field is illuminated with laser light at a frequency which coincides with that of a strong absorption feature in iodine, and with a linewidth which is narrow compared to the bandwidth of that absorption feature (of the order of 1 GHz). Doppler-shifted laser light, scattered by particles in the flow, is used to form dual images of the flow-field, only one of which is formed with filtered light. A comparison of the images yields information describing absorption and, implicitly, frequency shift and particle velocity. In these experiments, an injection-seeded, Q-switched pulsed Nd:YAG laser provided the required tuneable narrow-band illumination, with sufficiently short pulse duration (of the order of 10 ns) to resolve transient flow structures of interest. Thus, DGV delivers the instantaneous distribution of one velocity component over a two-dimensional plane slice of the flow region, as well as the useful qualitative flow visualisation which is available in the unprocessed images.

The configuration of the DGV apparatus for experiments on a drug delivery flow-field is shown schematically in Fig. 4. The plane of measurement is defined by the laser light sheet which is directed upstream along the nozzle centreline. The DGV imaging system was placed in a horizontal plane at an oblique angle to the nozzle axis. In this arrangement, the measurement is sensitive to an oblique component of the particle velocity vector. Assuming that the swirl velocities are small, axial velocity can be calculated directly from this component. The angle between the observation direction of the DGV imaging system and the nozzle axis determines the sensitivity of observed Doppler shift to axial velocity, and hence the velocity measurement range. In the configuration chosen for these experiments, the measurement range for axial velocity was approximately 0–910 m/s.

Velocity uncertainty in these measurements has been estimated by Quinlan (1999) as ±90 m/s or ±10% of maximum velocity, using an analysis developed by Thorpe et al. (1996). The basic spatial resolution is determined by CCD pixel size and camera magnification, which in this case result in a resolution of 0.12 mm. Velocity fields were smoothed in postprocessing with a 5×5 pixel median filter to give an effective spatial resolution of 0.6 mm.

Time resolution is governed by the repetition rate and duration of laser illumination and image acquisition. Because of the short duration of the transient flow, repetition rate limits the experiment to one velocity measurement per device actuation, so that a description of the developing unsteady flow-field is recorded over multiple instances of the flow. Variability in initial particle distribution, diaphragm rupture pressure, trigger timing

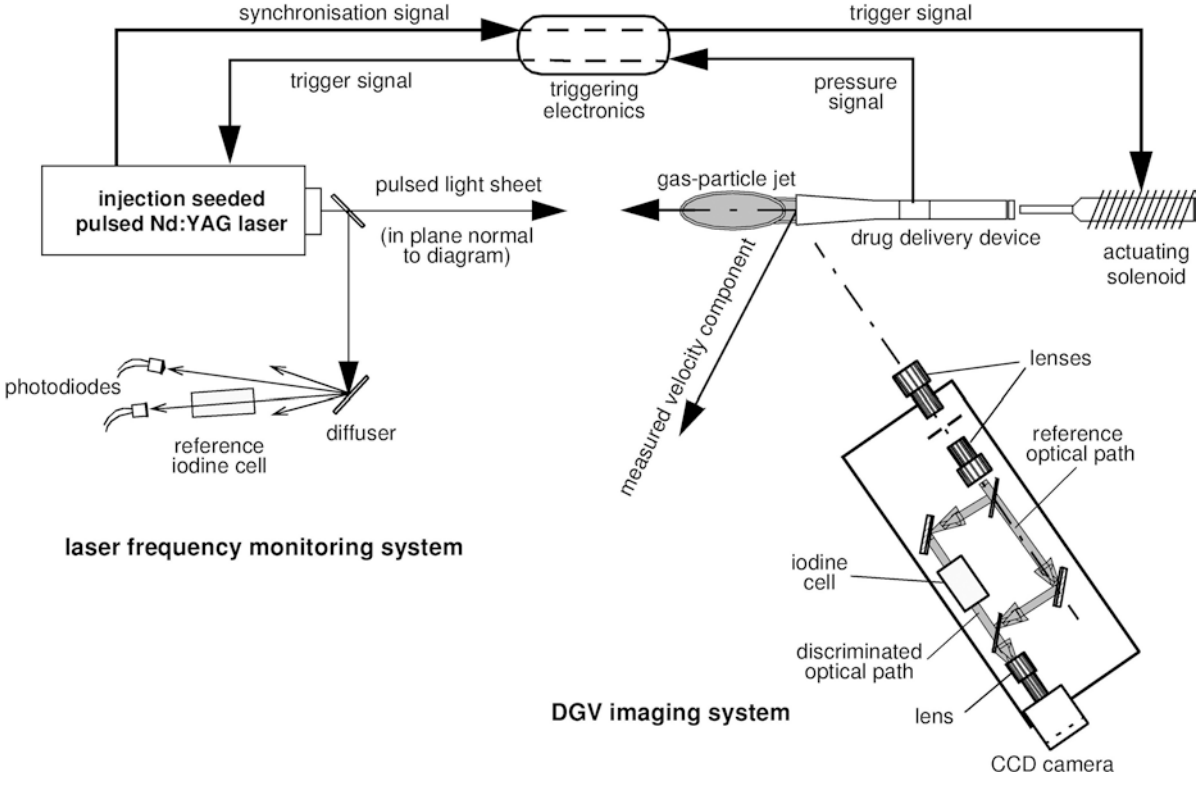

Fig. 4. Schematic of the DGV apparatus (not to scale)

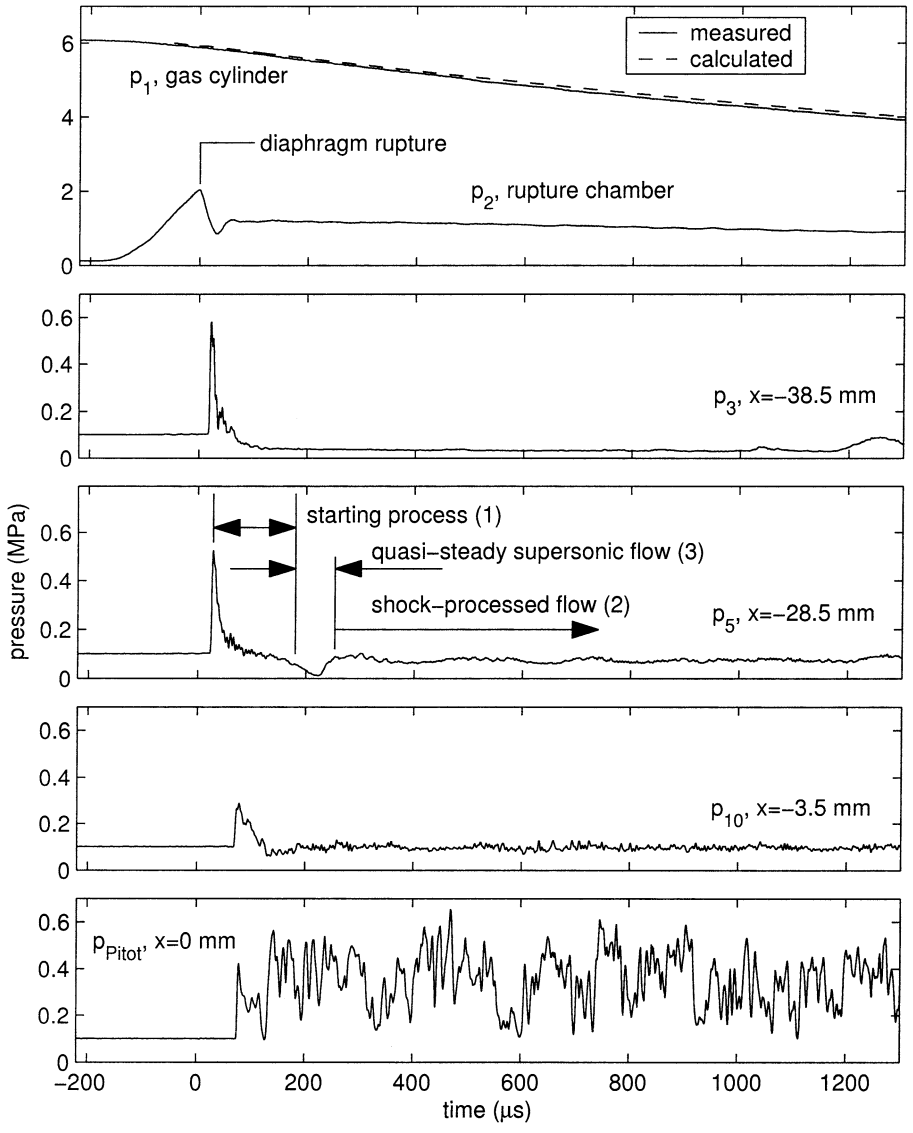

Fig. 5. Measured and calculated total pressure in the gas canister p_1, measured total pressure in the rupture chamber p_2, and static pressure at three nozzle wall locations p_3, p_5 and p_{10}. A Pitot pressure history p_{Pitot} measured at the centreline of the nozzle exit is also given. The calculations are based on the assumption of choked flow from the canister with an empirically determined discharge coefficient, and isentropic expansion in the canister

and the device actuation mechanism, as well as the turbulence of the flow, all add to the variability of the velocity measurement. In an assessment of repeatability over five nominally identical experiments, the standard deviation of delay from diaphragm rupture to velocity measurement was 8 μs, and the standard deviation of the velocity of the leading particles was 73 m/s. The laser pulse duration is approximately 10 ns, so that each individual velocity measurement is practically instantaneous.

Synchronisation of the pulsed illumination with the transient flow was achieved through electromechanical actuation of the prototype particle delivery device and monitoring of the flow history with a fast-response pressure transducer. The laser pulse repetition rate (10 Hz) and the camera readout time (of the order of 1 s) restricted the DGV system to a single measurement in each individual flow (with duration of the order of 5 ms). The vaccine delivery device tested had a transparent acrylic nozzle (Perspex, UK) of 2 mm wall thickness to enable visualisation and measurement of the flow within the nozzle. Unlike the particular device studied in schlieren experiments, the cross section of the nozzle for the DGV tests was circular and identical in profile to the nozzle for pressure measurements (shown in Fig. 2). The particle cassette was loaded with 1.0 mg of 4.7±0.4 μm (mean diameter, ± one standard deviation) polystyrene spheres (Duke Scientific, USA) which are representative of a payload of smaller pharmaceutical particles.

4
Results

4.1
Gas flow without particles

Measurements and predictions of the pressure histories in the canister (at location p_1) and rupture chamber (p_2) are shown in Fig. 5. In these regions of near-stagnant flow, the measured pressures closely approximate total pressure. The observed decay of canister pressure is consistent with a theoretical prediction based on the assumption of choked flow through the canister exit valve (labelled in Fig. 1). However, total pressure drops by a factor of approximately four between p_1 and p_2 due to shocks and viscous effects associated with flow through the valve.

Static pressure histories at nozzle measurement locations p_3, p_5 and p_{10} are also shown in Fig. 5. The key flow regimes are labelled on the p_5 pressure history. Flow is initiated by a primary shock, which opens a transient starting process of the type described by Smith (1966) and Amman and Reichenbach (1973) among others. This phase is followed by a quasi-steady supersonic flow, during which static pressure decreases as total pressure decays (mirroring the decay of rupture chamber pressure p_2). At position p_{10}, closer to the nozzle exit, the starting process is terminated by compression waves that initiate at the nozzle exit, coalesce and form a shock front that moves up the nozzle. This shock front first arrives at position p_5 and then at p_3 to terminate the quasi-steady supersonic flow.

A typical Pitot pressure measurement (p_{Pitot}) taken at the centreline of the nozzle exit is also shown in Fig. 5. Clearly, this pressure history is highly oscillatory, as a result of the shock cells in the over-expanded nozzle. These pressure profiles are typical of the over-expanded supersonic nozzle flows described by Higashino et al. (1991) and others.

Axial profiles of Mach number at various times after termination of the starting process (based on total-static and Pitot-static pressure measurements) are compared with the theoretical Mach number profile for steady isentropic quasi-one-dimensional supersonic flow (with the assumption of a choked throat) in Fig. 6. Total and static pressure measurements (p_2 and p_3 respectively) suggest that 500 μs after diaphragm rupture, the flow 38.5 mm upstream of the nozzle exit is supersonic and close to the isentropic ideal. Further downstream, however, the over-expanded nozzle flow is processed through an oblique shock system which induces flow separation. Consequently, the experimentally determined Mach number (determined from Pitot and static pressure) gradually falls from between 2 and 2.5 (23.5 mm upstream of the exit plane) to 1.5 at the exit plane. Sample error bars shown in Fig. 6 correspond to the standard deviation in Mach number calculated with the data ±50 μs from the time of interest. These error bars reflect the oscillatory Pitot pressure histories within the shock processed flow (as shown in Fig. 5). The Mach number in the downstream region of the nozzle decays with time as the shock system moves upstream.

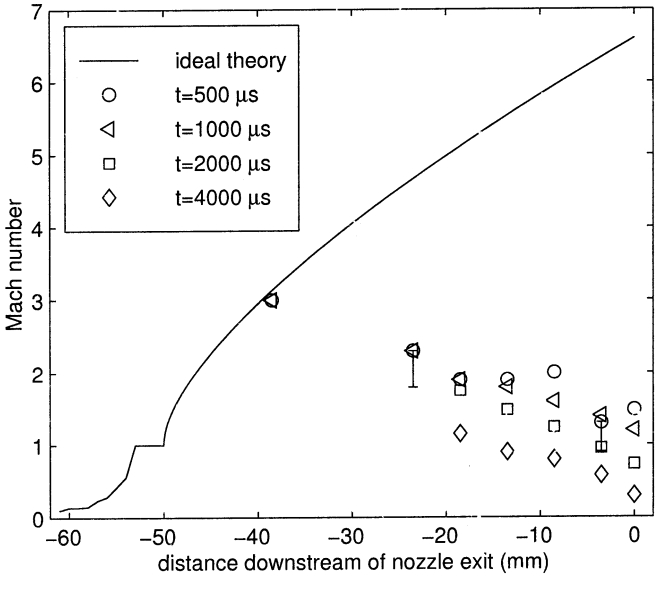

Fig. 6. Experimental and ideal axial Mach number within the conical nozzle of investigation. The profiles are provided after the starting process

Sequences of schlieren images such as the sample shown in Fig. 7 reveal the structure of the evolving flowfield with greater detail and clarity. Flow is from left to right. In the first image, 21 μs after diaphragm rupture (Fig. 7a) the density change designating a shock can be seen just within the left field of view. In the next image, 42 μs after diaphragm rupture, (Fig. 7b) the primary shock is followed by the interface (separating the helium driver and air driven gas) and an oblique shock front (secondary shocks). At this point in time, the oblique shock, which represents the termination point of the starting process, has not induced flow separation. In the next image (Fig. 7c), 90 μs later, the primary shock has exited the nozzle. The oblique shocks visible in Fig. 7b have evolved to form at least three oblique shock cells in Fig. 7c that have interacted with the boundary layer and separated the nozzle flow. Similar starting process shock structures have been observed and investigated by Gvozdeva and Zhilin (1977) and Britan and Vasilev (1986). This oblique shock system dominating the starting process exists as a result of over-expanded nozzle operation. Furthermore, the duration of the starting process is significantly longer than the definition adopted by Smith (1966) stated as the time taken for a steady flow characteristic to travel from the throat to a given location. The primary reason behind the discrepancy is that the operating conditions considered by Smith (1966) were hypersonic, with pressure and nozzle area ratios closer to the correctly expanded condition than those reported here.

Another distinctly singular oblique shock front evident 243 and 354 μs after diaphragm rupture (Fig. 7d and e respectively) is swept upstream from the exit plane after the primary shock has left the nozzle. This shock system forms the downstream boundary of the starting process and the subsequent quasi-steady supersonic flow. The oblique shocks, as in the starting process, separate the nozzle boundary layer. The shock angles and positions agree with the total pressure drop and shock positions deduced from the pressure measurements. The flow regimes identified and quantified in the pressure and schlieren measurements are mapped in a space-time diagram in Fig. 9 and are discussed in Sect. 5.

4.2
Gas and particle flow

A sequence of seven time-resolved DGV particle velocity measurements is shown in Fig. 8. They illustrate the instantaneous state of the particle flow at various stages in its development. The left column shows the measured velocity fields, while the corresponding images in the right column are partially processed images acquired in the course of each DGV experiment, and are useful qualitative visualisations of particle concentration distribution. Each pair comprising one velocity map and one particle

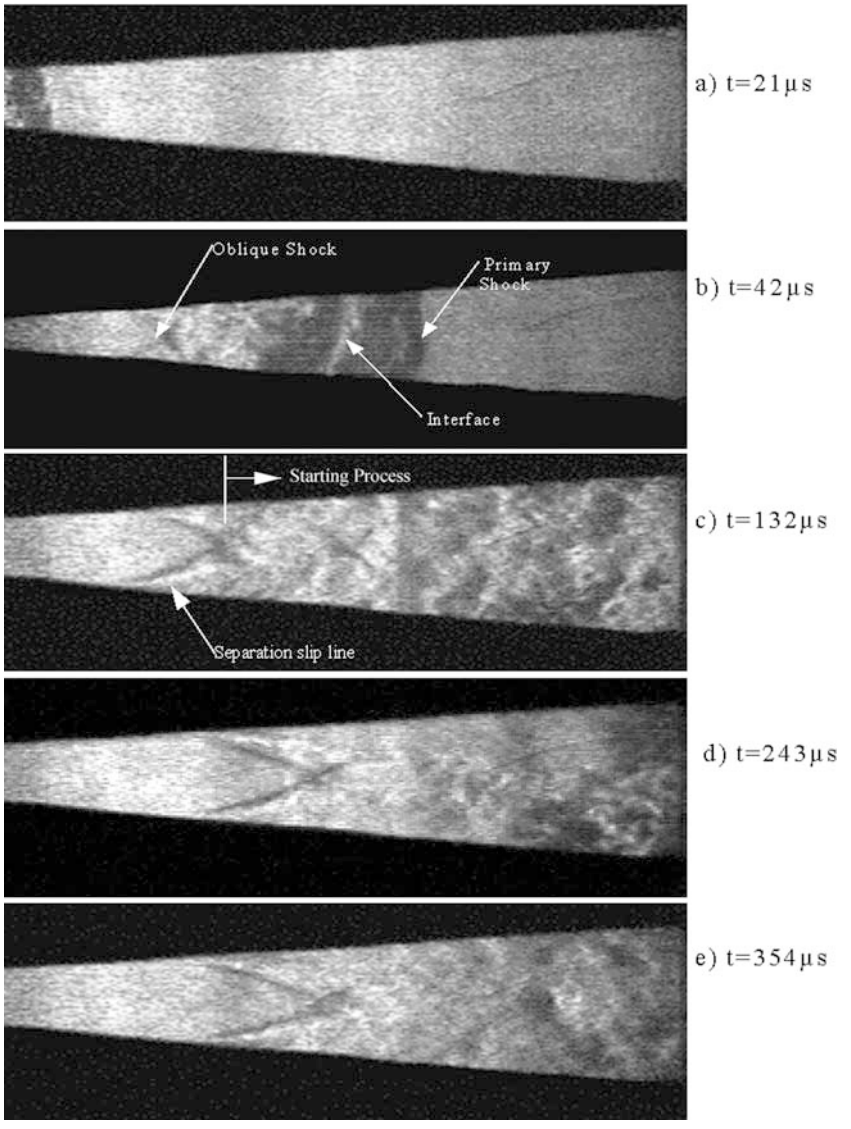

Fig. 7. Schlieren images within the square-section nozzle (profile shown in Fig. 2) at different time intervals after diaphragm rupture. There is no particle payload in these conditions

distribution image represents an instant in the history of a single unique flow; the similarity between velocity maps for t=146 and 147 μs is typical of the repeatability of the flow field and the measurement. The time t specified above each velocity map is measured from the beginning of flow in the nozzle. For areas very near the nozzle walls, and in a roughly elliptical band of each velocity map corresponding to an image of the obliquely viewed nozzle exit rim, optical effects render the velocity measurements unreliable. Consequently, no data are presented in these regions.

The early images capture the emergence of the first particles to be delivered to the target. They are led by a wide cloud of slow-moving particles at 200–400 m/s, which is followed by a stream of faster particles travelling at 650–800 m/s. The front of the slow-moving cloud is approximately planar as it approaches the nozzle exit. Once it has emerged, it develops a convex curved shape. The leading cloud expands radially as it travels, becoming wider than the nozzle exit. It is associated with the starting process in the gas flow. The high-velocity particle stream is embedded in the quasi-steady gas flow and pours into the leading cloud, probably imparting some momentum to it. This stream maintains a roughly constant diameter which is noticeably less than that of the nozzle exit. Within the quasi-steady stream, velocity is high and roughly uniform within a core region of some 8–10 mm in diameter. Some velocity maps (e.g. those presented for t=147 and 177 μs) show that the core of the high-speed particle flow breaks away from the nozzle wall 15–30 mm upstream of the exit. This is consistent with the shock-induced flow separation observed in schlieren experiments (Fig. 7).

The particle concentration images display interesting structure in the particle distribution. The concentration of drug particles in the leading cloud is usually high, and varies smoothly. Concentration is typically lower in the high-speed stream which follows, but it is interspersed with long, slender regions of high concentration which are oriented approximately parallel to the nozzle axis.

After the leading cloud has passed from view, around 200 μs after the initiation of flow, the high-velocity stream remains essentially unchanged for a further 100 μs. The velocity of the particle jet then begins to decay appreciably, falling to 400 m/s after 1 ms, at which point particle concentration (indicated by the reference images) is so low

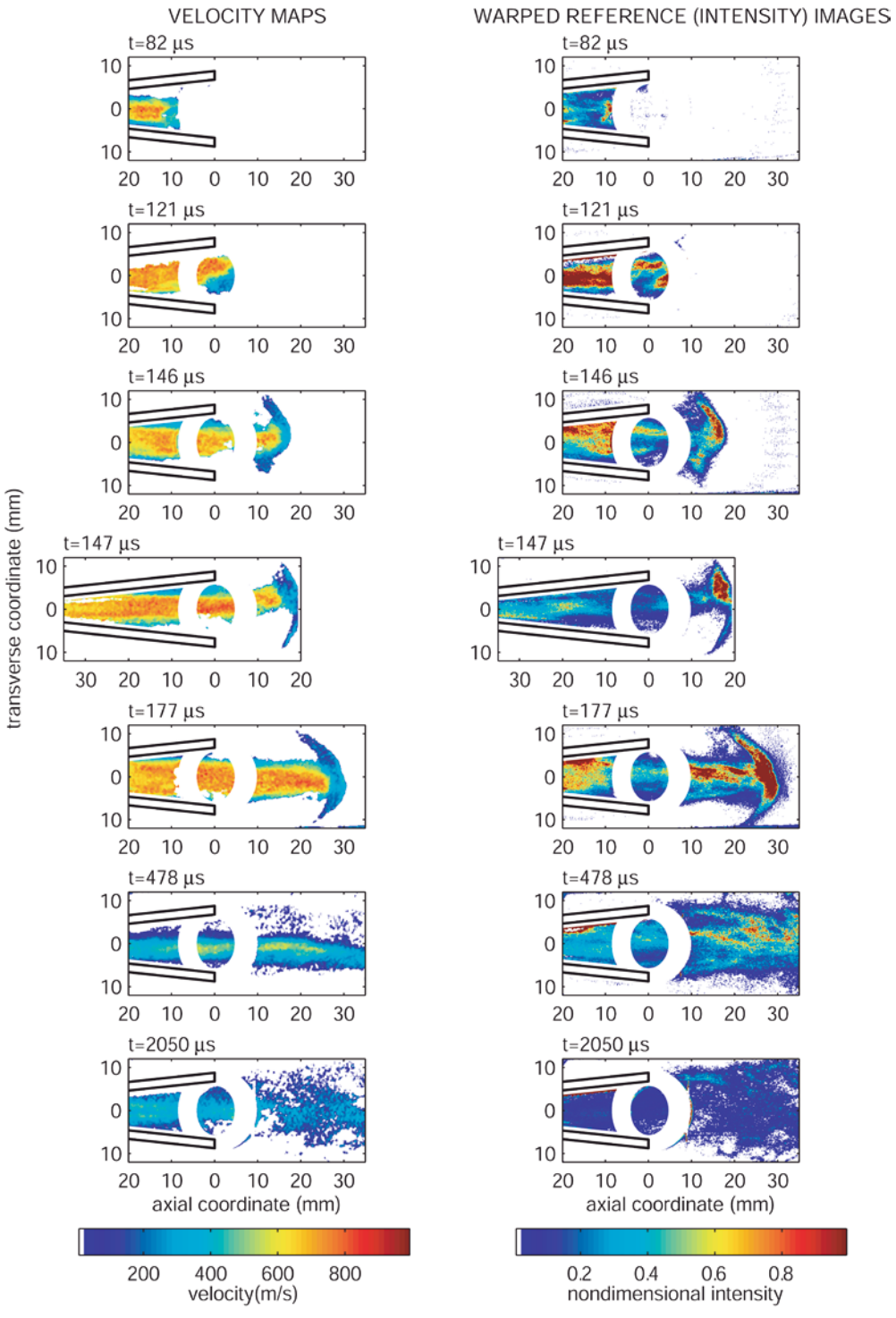

Fig. 8. Time-resolved DGV particle velocity measurements. Images in the left column are measured instantaneous velocity fields. The corresponding images on the right hand side are partially processed flow-field images, giving qualitative visualisations of particle concentration distribution

that particles are hardly detectable above the background. In this period, decaying total pressure leads to reduced gas velocities in the nozzle, and the last particles are being flushed from the pharmaceutical storage cassette.

5 Discussion

Data from the pressure measurements, schlieren and DGV images have been combined in the form of a space-time (x-t) diagram (Fig. 9). The gas flow has been broadly categorised into three labelled flow regimes:

1. The starting process.
2. Shock-processed flow. Gas flow processed by the oblique shock system swept upstream of the nozzle exit as a result of over-expanded operation.
3. Quasi-steady supersonic flow.

Note the well-defined secondary shock immediately downstream of the interface within the starting process. The effect of the gas flow-field regimes on particle acceleration is illustrated by sample particle trajectories obtained with DGV. Firstly, a significant proportion of

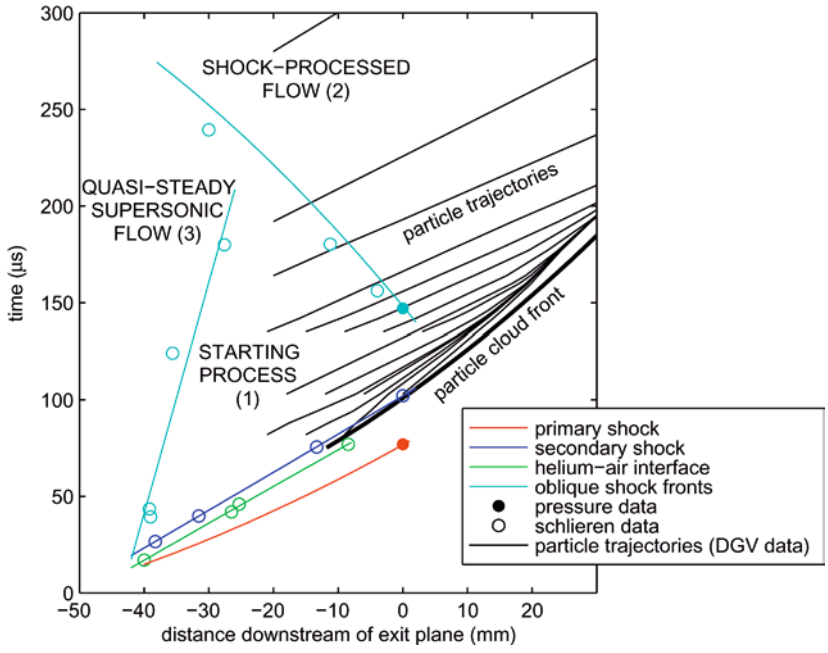

Fig. 9. A space-time (x-t) diagram of the gas flow regimes and sample particle trajectories within the prototype converging-diverging nozzle

the particles are accelerated within the starting process until they decelerate as they reach the secondary shock and helium-air interface. These particles are those entrained within the initial 200–400 m/s cloud attached to the nozzle wall observed in the DGV images in Fig. 8. Another fraction of particles do not reach the secondary shock, but are processed firstly by the oblique shocks and separated jet within the starting process (noted as region 1 in Fig. 9) and then the upstream-moving oblique shock which defines the separated flow within region 2. Finally, a component of the payload is accelerated within the quasi-steady flow (region 3), before passing through the quasi-stationary oblique shock front into the shock-processed, separated flow of region 2. This is indicated by the orientation of trajectories on the x-t diagram for particles which reach the nozzle exit approximately 250 μs after the beginning of flow, or later. This acceleration path leads to the highest particle velocities of 800 m/s, confined to a defined, separated jet of 8–10 mm diameter. Incidentally, observations of the particle distribution delivered from the nozzle into agar gel and skin sections are consistent with these free jet measurements; within an overall target diameter of ∼13 mm there is a central 8–10 mm diameter "core" which consists of a higher number of particles that have penetrated further into the target.

The general implications of these findings (within a prototype system) are that entrainment of particles within the starting process and over-expanded flows — that is, in regimes of temporally and spatially non-uniform flow — gives rise to variations in particle velocity and concentration. Therefore, if uniform spatial and velocity distributions are required in the intradermal delivery of certain pharmaceutical agents, then it is desirable to generate a correctly expanded, attached steady gas flow within which the particle payload is entrained. One concept configured for controlled particle delivery applications is the contoured shock tube (CST) described by Kendall (2002). These nominally uniform particle penetration characteristics warrant the utility of the CST as an essential research tool in fundamental studies that require the uncoupling of delivery system and biological variability. For instance, particle depth measurements have been obtained for a range of particle densities and impact velocities targeting human skin at different sites of the body (Kendall et al. 2001; Kendall et al. 2000). Similarly, the particle impact momentum requirements for delivery to defined locations of the buccal mucosa has also been determined with CST systems (Mitchell et al. 2003).

6 Conclusions

The transient gas and particle dynamics within a prototype transonic converging-diverging supersonic nozzle have been characterised by experiment. Static and Pitot pressure measurements and schlieren images were used to evaluate the gas flow-field. Measurements of the transient particle positions and velocities have been obtained with Doppler global velocimetry (DGV).

It has been established in the prototype system that total pressure losses and large nozzle area ratios have resulted in over-expanded nozzle operation. This has led to gas and particle flow non-uniformities generated by oblique shock systems, along with associated flow separation within the starting process and the subsequent quasi-steady supersonic flow. In some applications of this form of needle-free pharmaceutical agent delivery to the skin, a tighter control of the particle impact momentum distribution may be required. In this case, nozzles in which a correctly expanded, attached, and steady gas flow entrains all the particle payload may be used.

References

Ainsworth RW, Thorpe SJ, Manners RJ (1997) A new approach to flow-field measurement—a view of Doppler global velocimetry techniques. Int J Heat Fluid Flow 18:116–130

Amman HO, Reichenbach H (1973) Unsteady flow phenomena in shock-tube nozzles. In: Bershader D, Griffith W (eds) Recent developments in shock tube research. Proceedings of the ninth international shock tube symposium. Stanford University Press, Stanford

Bellhouse BJ, Sarphie DF, Greenford JC (1994) Needless syringe using supersonic gas flow for particle delivery. International patent Wo94/24263

Britan AB, Vasilev EI (1986) Investigation of the starting process in the shaped nozzle of a large diameter shock tube. (translation by Plenum, New York from Russian Mekhanika Zhidkosti I Gaza) Fluid Dyn 21:5

Burkoth TL, Bellhouse BJ, Hewson G, Longridge DJ, Muddle AG, Sarphie DF (1999) Transdermal and transmucosal powdered drug delivery. Crit Rev Ther Drug 16(4)331–384

Chen DX, Endres RL, Erickson CA, Weis K F, McGregor MW, Kawaoka Y, Payne LG (2000) Epidermal immunization by a needle-free powder delivery technology: immunogenicity of influenza vaccine and protection in mice. Nat Med 6:1187–1190

Gvozdeva LG, Zhilin YV (1977) Formation of a quasistationary jet within a nozzle during its start-up. (translation by Plenum, New York from Russian Mekhanika Zhidkosti I Gaza) Fluid Dyn 1:77–82

Higashino F, Matsuo S, Tsuyuki T (1991) Oscillation of oblique shock waves generated in a two dimensional asymmetric nozzle. SAE Transactions 100:2254–2262

Kendall MAF, Wrighton-Smith PJ, Bellhouse BJ (2000) Transdermal ballistic delivery of micro-particles: investigation into skin penetration. World congress on medical physics and biomedical engineering, Chicago, July 2000

Kendall MAF, Mitchell TJ, Hardy MP, Bellhouse BJ (2001) The ballistic delivery of high-density, high-velocity micro-particles into excised human skin. ASME bioengineering conference, Snowbird, UT, 27–30 June

Kendall MAF (2002) The delivery of particulate vaccines and drugs to human skin with a practical, hand-held shock tube-based system. Shock Waves 12:23–30

Lesinski GB, Smithson SL, Srivastava N, Chen DX, Widera G, Westerink J (2001) A DNA vaccine encoding a peptide mimic of *Streptococcus pneumoniae* serotype 4 capsular polysaccharide induces specific anti-carbohydrate antibodies in Balb/c mice. Vaccine 19:1717–1726

Mitchell TM, Kendall MAF, Bellhouse BJ (2003) A ballistic study of micro-particle penetration to the oral mucosa. International Journal of Impact Engineering, 28:581–599

Quinlan NJ (1999) Gas and particle dynamics in transdermal powdered drug delivery. DPhil. Thesis, Engineering Science, University of Oxford

Quinlan NJ, Kendall MAF, Bellhouse BJ, Ainsworth RW (2001) Investigations of gas-particle flow in first generation dermal PowderJect needle-free drug delivery systems. Shock Waves 10(6):395–404

Sanford JC, Wolf ED, Allen NK (1990) Method for transporting substances in to living cells and tissues and apparatus therefore. US Patent 4,945,050

Smith CE (1966) The starting process in a hypersonic nozzle. J Fluid Mech 24(4):625–640

Thorpe SJ, Ainsworth RW, Manners RJ (1996) Time-averaged free-jet measurements using Doppler global velocimetry. ASME symposium on laser anemometry and experimental and numerical flow visualisation. San Diego

Thorpe SJ, Quinlan NJ, Ainsworth RW (2000) Development of a Nd:YAG-based Doppler global velocimetry system and application to unsteady flows. Opt Laser Eng 32:7–8